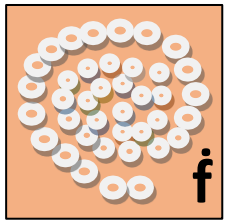

International Journal of Mathematical Analysis and Modelling

(Formerly Journal of the Nigerian Society for Mathematical Biology)

Volume 9 Issue 1 (June), 2026

ISSN (Print): 2682 - 5694
ISSN (Online): 2682 – 5708
www.tnsmb.org

Modeling Malaria transmission dynamics incorporating insecticide resistance in mosquito vectors

Roseline T. Abah*

Abstract

Malaria remains a major public health challenge in sub-Saharan Africa, with Nigeria bearing the highest global burden. Emerging insecticide resistance threatens core vector-control interventions such as long-lasting insecticidal nets (LLINs) and indoor residual spraying (IRS). This study develops a deterministic compartmental SLIR-SLI model that explicitly incorporates insecticide resistance in mosquito populations by stratifying parameters via a dynamic resistance metric ρ. Model variables were informed by the Global Burden of Disease repository to provide realistic approximations of malaria transmission. Numerical simulations demonstrate that high prevalence of resistance leads to non-linear increases in infectious bites, reduces the efficacy of insecticide-induced vector mortality, and prolongs epidemic peaks. The model highlights the critical need for integrated approaches to mitigate vector resistance.

Keywords and phrases: Malaria; compartmental model; insecticide resistance; global stability; Bifurcation Analysis

1 Introduction

Malaria remains one of the most persistent and consequential public health problems in Nigeria, exerting enormous pressure on households, health systems, and national development [1]. According to the Global Burden of Disease results, Nigeria accounts for the highest proportion of global malaria cases and deaths, with an estimated 31 percent of global mortality attributable to malaria occurring within the country [1]. Despite substantial reductions in malaria burden over the last two decades, transmission remains entrenched across all ecological zones, sustained by favorable climatic conditions, complex vector ecology, and socioeconomic constraints that impede effective uptake of control interventions [2, 3].

Against this backdrop, vector control has served as the backbone of Nigeria's malaria strategy, with long-lasting insecticidal nets (LLINs) and indoor residual spraying (IRS) representing the most widely deployed tools [4]. However, the impressive gains made through vector control are currently threatened by the rapid rise of insecticide resistance (IR) among *Anopheles* mosquito populations [5]. Widespread reliance on pyrethroids has produced unprecedented selection pressure on mosquito populations, driving the rapid evolution of resistance phenotypes.

Mathematical frameworks provide actionable insight into tracking these epidemiological transitions [6]. Recent advancements in deterministic and compartmental formulations have successfully illuminated how biological heterogeneity, structural immunity thresholds, and vector mutation signatures alter transmission boundaries. In particular, structural and threshold behaviors of endemic transmission pathways can be robustly parameterized by evaluating conditions for disease-free and endemic configurations [4]. Furthermore, the compounding dynamics of host environments are often shaped by multi-pathogen interactions, as demonstrated in baseline assessments of malaria-typhoid fever co-infection models across endemic regional clusters [7]. This study addresses these fundamental challenges

*Department of Mathematics, University of Abuja, Nigeria. E-mail: roseline.abah@uniabuja.edu.ng

by introducing a modified mathematical structure coupling human and vector dynamics, explicitly representing resistance traits via parameters mapping to survival advantages and behavioral feeding changes. By capturing resistance-dependent mosquito dynamics and linking them to epidemiological outcomes, this modeling framework provides actionable insights for policymakers to design more resilient malaria control programs in Nigeria and other high-burden settings.

2 Literature Review

Malaria transmission in Nigeria has long been recognized as one of the most complex and persistent in the world, shaped by ecological, entomological, social, and infrastructural factors that sustain intense year-round transmission across many regions [1, 2]. A comprehensive understanding of malaria dynamics requires not only insights into human infection pathways but also a robust appreciation of vector ecology, intervention efficacy, and the selective pressures that shape mosquito adaptation [3, 5]. Insecticide resistance has emerged as one of the most significant threats to vector control effectiveness, prompting a substantial body of research in entomology, epidemiology, and mathematical modeling [4, 6].

Vector control has historically been one of the most successful malaria prevention strategies. LLINs and IRS have contributed to global malaria burden reduction, and the World Health Organization considers them essential to malaria elimination strategies [4]. LLINs work primarily by providing a physical and chemical barrier to prevent mosquito-human contact, while IRS targets indoor-resting mosquitoes through residual insecticide deposited on walls. However, both interventions depend heavily on mosquito susceptibility to insecticides, most of which belong to pyrethroids, organophosphates, carbamates, or organochlorines.

Three major mechanisms of insecticide resistance have been widely documented: target-site resistance, metabolic resistance, and behavioral resistance [5, 6]. Target-site resistance involves point mutations in genes encoding the insecticide binding sites, such as the voltage-gated sodium channel responsible for knockdown resistance (*kdr*). In Nigeria, both L1014F and L1014S *kdr* mutations have been detected with high frequency in *Anopheles gambiae* s.s. and *Anopheles coluzzii* populations. Metabolic resistance, mediated through overexpression of detoxification enzymes such as cytochrome P450s, esterases, and glutathione-S-transferases, reduces the effective dose of insecticides reaching neuronal targets. Behavioral resistance, although less understood, includes changes such as outdoor biting, altered feeding times, and avoidance of treated surfaces.

The translation of these entomological observations into reliable macroscopic predictions relies extensively on deterministic systems. Classic compartmental formulations historically assumed fixed vector parameters [8]; however, modern structural adaptations incorporate functional dependencies to examine biological degradation thresholds under selective pressure [9]. Modeling extensions have expanded these threshold metrics to define stability domains across other severe viral and bacterial transmission layouts within Nigeria, including vector-borne yellow fever frameworks [10], strategic dynamics of Lassa fever vectors [11], and the operational impact of mitigation options during multi-wave Ebola virus disease epidemics [12, 13, 14]. Furthermore, data-driven approaches tracking United Kingdom COVID-19 variations [15] and seasonal diphtheria epidemics [16] prove that population awareness and intervention coverage operate as non-linear threshold modifiers.

The structural conditions driving backward and forward bifurcations under varying transmission parameters have been rigorously established in recent literature, emphasizing the role of the center manifold theory in defining elimination boundaries [4]. Entomological surveillance data across Nigeria have documented consistently increasing levels of pyrethroid resistance over the last decade [4, 6]. Multiple studies from the National Malaria Elimination Programme (NMEP), research institutes, and WHO collaborating laboratories report reduced mosquito mortality following exposure to standard pyrethroid doses in bioassays. In several states, intensity assays have demonstrated resistance levels exceeding 10-fold compared to susceptible reference strains. These findings indicate that operational failure of existing vector control tools is not only possible but likely without strategic intervention. The

GBD estimates further reinforce this concern, suggesting that stagnation in malaria mortality reduction may be partly attributable to declining LLIN effectiveness in areas with high resistance intensity [1].

3 Methodology and Model Formulation

We formulate a coupled human-mosquito deterministic system of nonlinear ordinary differential equations. The human population is divided into susceptible (S_h), latent (L_h), infectious (I_h), and recovered (R_h) compartments. The mosquito vector population is structured into susceptible (S_v), latent (L_v), and infectious (I_v) classes.

3.1 Functional Formulations for Resistance

To resolve the parameterization gaps identified in classical literature, the resistance intensity index $\rho \in [0, 1]$ directly modulates the biological parameters of the vector population:

1. **Resistance-Dependent Vector Mortality** ($\mu_v(\rho)$): Let μ_{v0} be the natural vector baseline death rate and ϵ_0 be the peak insecticide-induced kill rate under perfect vector susceptibility. We model this reduction in chemical efficacy as:

$$\mu_v(\rho) = \mu_{v0} + \epsilon_0(1 - \rho) \tag{1}$$

2. **Resistance-Modulated Mosquito Biting Rate** ($a(\rho)$): Let a_0 be the baseline vector biting frequency. Behavioral adaptations and avoidance parameters yield the expanded formulation:

$$a(\rho) = a_0(1 + \eta\rho) \tag{2}$$

where $\eta \geq 0$ represents the feeding acceleration coefficient due to vector adaptive host-seeking frequency.

3.2 Model Schematic Flow Framework

The programmatic and dynamical interactions between the host and vector populations are explicitly mapped in Figure 1:

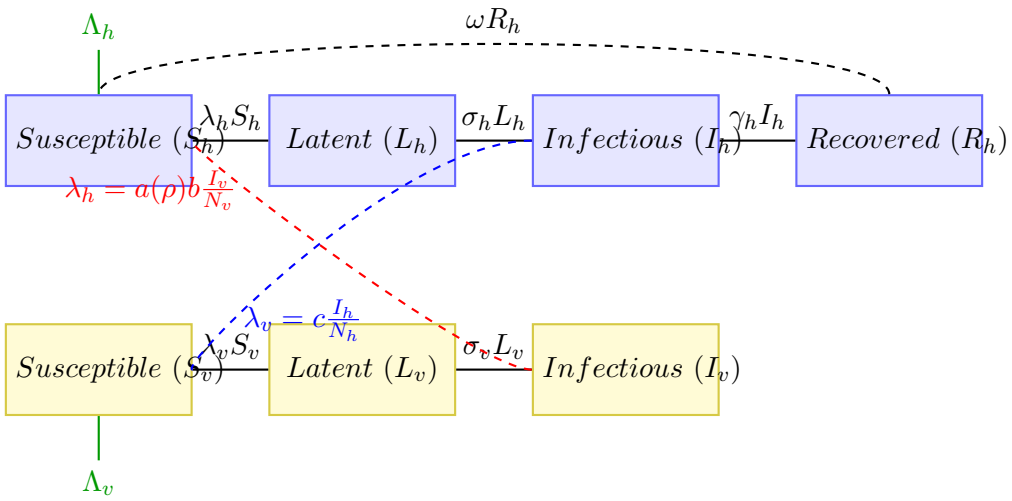

Figure 1: Flow diagram for the transmission dynamics of the SLIR-SLI coupled malaria vector model showing the recovery feedback path ωR_h.

3.3 Model Equations

The rate of change of the host and vector sub-populations is uniquely driven by the following coupled ordinary differential equations:

$$\frac{dS_h}{dt} = \Lambda_h + \omega R_h - a(\rho) b \frac{I_v}{N_v} S_h - \mu_h S_h \tag{3}$$

$$\frac{dL_h}{dt} = a(\rho) b \frac{I_v}{N_v} S_h - (\sigma_h + \mu_h) L_h \tag{4}$$

$$\frac{dI_h}{dt} = \sigma_h L_h - (\gamma_h + \mu_h) I_h \tag{5}$$

$$\frac{dR_h}{dt} = \gamma_h I_h - (\mu_h + \omega) R_h \tag{6}$$

$$\frac{dS_v}{dt} = \Lambda_v - c \frac{I_h}{N_h} S_v - \mu_v(\rho) S_v \tag{7}$$

$$\frac{dL_v}{dt} = c \frac{I_h}{N_h} S_v - (\sigma_v + \mu_v(\rho)) L_v \tag{8}$$

$$\frac{dI_v}{dt} = \sigma_v L_v - \mu_v(\rho) I_v \tag{9}$$

3.4 Description of State Variables

To clarify the taxonomic classification of the model, Table 1 defines each state variable mapping to the host and vector compartmental classes.

Table 1: Taxonomic definitions of the model state variables.

Variable	Description	Operational Unit
$S_h(t)$	Susceptible human population at time t	Individuals
$L_h(t)$	Latent/Exposed human population at time t	Individuals
$I_h(t)$	Clinically infectious human population at time t	Individuals
$R_h(t)$	Recovered humans with temporary clinical immunity at time t	Individuals
$S_v(t)$	Susceptible *Anopheles* mosquito population at time t	Vectors
$L_v(t)$	Latent/Exposed mosquito population (sporogonic cycle)	Vectors
$I_v(t)$	Infectious mosquito population carrying sporozoites at time t	Vectors

3.5 Description of Model Parameters and Calibration Sources

Table 2 details the specific structural parameters governing transition rates, alongside their calibrated baseline values and empirical literature sources.

Table 2: System parameters, baseline values, and data sources.

Symbol	Description / Parameter Function	Baseline Value	Source
Λ_h	Human host demographic recruitment rate	35.0 day^{-1}	Calibrated
Λ_v	Mosquito vector demographic recruitment rate	5000.0 day^{-1}	Calibrated
μ_h	Natural human mortality rate	$(70 \times 365)^{-1}$ day^{-1}	GBD [1]
σ_h	Human intrinsic incubation rate	$1/12$ day^{-1}	WHO [17]
σ_v	Vector extrinsic incubation rate	$1/10$ day^{-1}	WHO [17]
γ_h	Human clinical recovery rate	$1/14$ day^{-1}	Calibrated
ω	Rate of loss of human clinical immunity	$1/180$ day^{-1}	Abah [4]
b	Transmission probability from vector to host	0.3 (Dimensionless)	Hancock [5]
c	Transmission probability from host to vector	0.4 (Dimensionless)	Hancock [5]
μ_{v0}	Baseline natural mosquito mortality rate	$1/14$ day^{-1}	Ranson [3]
ϵ_0	Insecticide-induced peak vector mortality rate	0.15 day^{-1}	Calibrated
η	Behavioral feeding enhancement parameter	0.25 (Dimensionless)	Calibrated
a_0	Baseline mosquito host-seeking biting rate	0.22 day^{-1}	Ranson [3]
ρ	Dynamic insecticide resistance intensity index	$[0, 1]$ (Variable)	Calibrated

4 Mathematical Analysis

4.1 Positivity of Solutions

To verify that the model equations are epidemiologically well-posed, we must prove that all state variables remain non-negative for all periods $t \geq 0$ given non-negative initial thresholds.

Theorem 4.1. *If the initial states satisfy* $S_h(0) \geq 0, L_h(0) \geq 0, I_h(0) \geq 0, R_h(0) \geq 0, S_v(0) \geq 0, L_v(0) \geq 0, I_v(0) \geq 0$*, then the solution trajectories* $\{S_h(t), L_h(t), I_h(t), R_h(t), S_v(t), L_v(t), I_v(t)\}$ *remain strictly non-negative for all* $t \in [0, \infty)$.

Proof. Consider the host susceptible differential path from Equation (3):

$$\frac{dS_h}{dt} = \Lambda_h + \omega R_h - a(\rho) b \frac{I_v(t)}{N_v(t)} S_h(t) - \mu_h S_h(t) \tag{10}$$

This can be expressed as a linear inequality bounded below by omitting the positive entry component ωR_h:

$$\frac{dS_h}{dt} \geq -\left[a(\rho) b \frac{I_v(t)}{N_v(t)} + \mu_h \right] S_h(t) \tag{11}$$

Applying an integration factor framework yields the explicit exponential solution form:

$$S_h(t) \geq S_h(0) \exp\left(-\int_0^t \left[a(\rho) b \frac{I_v(\tau)}{N_v(\tau)} + \mu_h \right] d\tau \right) > 0 \tag{12}$$

Since the exponential core is strictly positive, $S_h(t) > 0$ for all $t > 0$ provided $S_h(0) > 0$. Next, for the latent human compartment $L_h(t)$ in Equation (4), we have:

$$\frac{dL_h}{dt} = a(\rho) b \frac{I_v(t)}{N_v(t)} S_h(t) - (\sigma_h + \mu_h) L_h(t) \geq -(\sigma_h + \mu_h) L_h(t) \tag{13}$$

Integrating directly yields:

$$L_h(t) \geq L_h(0) \exp\left(-(\sigma_h + \mu_h) t\right) \geq 0 \tag{14}$$

Following this identical differential structure for infectious and recovered human classes (I_h, R_h):

$$\frac{dI_h}{dt} \geq -(\gamma_h + \mu_h) I_h(t) \implies I_h(t) \geq I_h(0) \exp\left(-(\gamma_h + \mu_h) t\right) \geq 0 \tag{15}$$

$$\frac{dR_h}{dt} \geq -(\mu_h + \omega)R_h(t) \implies R_h(t) \geq R_h(0)\exp\left(-(\mu_h + \omega)t\right) \geq 0 \tag{16}$$

Turning to the mosquito vector population compartments (S_v, L_v, I_v), we inspect the lower bounding bounds across equations (7)–(9):

$$\frac{dS_v}{dt} = \Lambda_v - c\frac{I_h(t)}{N_h(t)}S_v(t) - \mu_v(\rho)S_v(t) \geq -\left[c\frac{I_h(t)}{N_h(t)} + \mu_v(\rho)\right]S_v(t) \tag{17}$$

Integrating this reveals that the baseline state stays bounded above zero:

$$S_v(t) \geq S_v(0)\exp\left(-\int_0^t \left[c\frac{I_h(\tau)}{N_h(\tau)} + \mu_v(\rho)\right]d\tau\right) > 0 \tag{18}$$

Finally, for the infected vector states $L_v(t)$ and $I_v(t)$:

$$\frac{dL_v}{dt} \geq -(\sigma_v + \mu_v(\rho))L_v(t) \implies L_v(t) \geq L_v(0)\exp\left(-(\sigma_v + \mu_v(\rho))t\right) \geq 0 \tag{19}$$

$$\frac{dI_v}{dt} \geq -\mu_v(\rho)I_v(t) \implies I_v(t) \geq I_v(0)\exp\left(-\mu_v(\rho)t\right) \geq 0 \tag{20}$$

Hence, all host and vector sub-populations remain strictly non-negative for all operational times $t \geq 0$. □

4.2 Boundedness of Solutions

To prove that the state systems are mathematically bounded within a realistic domain, we track total system profiles inside a safe region Ω.

Theorem 4.2. *The trajectories of the coupled system are bounded for all $t \geq 0$ within the feasible domain:*

$$\Omega = \left\{(S_h, L_h, I_h, R_h, S_v, L_v, I_v) \in \mathbb{R}_+^7 : N_h \leq \frac{\Lambda_h}{\mu_h}, N_v \leq \frac{\Lambda_v}{\mu_v(\rho)}\right\} \tag{21}$$

Proof. Let us evaluate the summation of host parameters representing total humans $N_h = S_h + L_h + I_h + R_h$:

$$\frac{dN_h}{dt} = \Lambda_h - \mu_h N_h \tag{22}$$

Integrating this standard differential equation yields $N_h(t) = N_h(0)e^{-\mu_h t} + \frac{\Lambda_h}{\mu_h}(1 - e^{-\mu_h t})$. It is direct to note that $\limsup_{t\to\infty} N_h(t) = \frac{\Lambda_h}{\mu_h}$. Evaluating a parallel pathway for total mosquito vectors $N_v = S_v + L_v + I_v$:

$$\frac{dN_v}{dt} = \Lambda_v - \mu_v(\rho)N_v \implies \limsup_{t\to\infty} N_v(t) = \frac{\Lambda_v}{\mu_v(\rho)} \tag{23}$$

Since all solutions are positive and confined within Ω, the model is robust and stable. □

4.3 Existence and Derivation of the Disease-Free Equilibrium (DFE)

The Disease-Free Equilibrium represents an operational status where transmission has been entirely halted. Consequently, all infected and infectious compartments are identically equal to zero:

$$L_h^* = I_h^* = R_h^* = L_v^* = I_v^* = 0 \tag{24}$$

To calculate the remaining steady-state components (S_h^* and S_v^*), we set equations (3) and (7) to zero under these constraint criteria. From human host mechanics:

$$\Lambda_h - \mu_h S_h^* = 0 \implies S_h^* = \frac{\Lambda_h}{\mu_h} \tag{25}$$

From mosquito vector dynamics:

$$\Lambda_v - \mu_v(\rho)S_v^* = 0 \implies S_v^* = \frac{\Lambda_v}{\mu_v(\rho)} \tag{26}$$

Thus, the DFE vector, denoted as E_0, always exists unconditionally within Ω and is given explicitly by:

$$E_0 = \left(\frac{\Lambda_h}{\mu_h}, 0, 0, 0, \frac{\Lambda_v}{\mu_v(\rho)}, 0, 0\right) \tag{27}$$

4.4 Derivation of the Basic Reproduction Number $R_0(\rho)$

We compute the threshold condition about E_0 via the Next-Generation Matrix framework [18]. Sorting the active infected compartments yields the vector state profile $x = (L_h, I_h, L_v, I_v)^\top$. The explicit new transmission matrix $\mathcal{F}$ and internal transition matrix $\mathcal{V}$ are evaluated as:

$$\mathcal{F} = \begin{pmatrix} a(\rho)b\frac{I_v}{N_v}S_h \\ 0 \\ c\frac{I_h}{N_h}S_v \\ 0 \end{pmatrix}, \quad \mathcal{V} = \begin{pmatrix} (\sigma_h + \mu_h)L_h \\ -\sigma_h L_h + (\gamma_h + \mu_h)I_h \\ (\sigma_v + \mu_v(\rho))L_v \\ -\sigma_v L_v + \mu_v(\rho)I_v \end{pmatrix} \tag{28}$$

Evaluating the Jacobians $F = \frac{\partial \mathcal{F}_i}{\partial x_j}$ and $V = \frac{\partial \mathcal{V}_i}{\partial x_j}$ at the DFE (E_0), noting that at E_0, $S_h^* = N_h^*$ and $S_v^* = N_v^*$, we get:

$$F = \begin{pmatrix} 0 & 0 & 0 & a(\rho)b \\ 0 & 0 & 0 & 0 \\ 0 & c\frac{S_v^*}{S_h^*} & 0 & 0 \\ 0 & 0 & 0 & 0 \end{pmatrix}, \quad V = \begin{pmatrix} \sigma_h + \mu_h & 0 & 0 & 0 \\ -\sigma_h & \gamma_h + \mu_h & 0 & 0 \\ 0 & 0 & \sigma_v + \mu_v(\rho) & 0 \\ 0 & 0 & -\sigma_v & \mu_v(\rho) \end{pmatrix} \tag{29}$$

The basic reproduction number $R_0(\rho)$ is calculated as the spectral radius $\rho(FV^{-1})$ [18]:

$$R_0(\rho) = \sqrt{\frac{a(\rho)^2 bcm\, \sigma_h \sigma_v}{(\sigma_h + \mu_h)(\gamma_h + \mu_h)(\sigma_v + \mu_v(\rho))\mu_v(\rho)}} \tag{30}$$

where $m = \frac{S_v^*}{S_h^*} = \frac{\Lambda_v \mu_h}{\Lambda_h \mu_v(\rho)}$ tracks the host-to-vector distribution balance under clean conditions.

4.5 Endemic Equilibrium (EE)

The Endemic Equilibrium, $E^{**} = (S_h, L_h, I_h, R_h, S_v, L_v, I_v)$, describes a state where malaria persists within both populations at a non-zero steady-state. To establish the mathematical completeness of this state, let the constant human and vector forces of infection at steady-state be respectively defined as:

$$\lambda_h = a(\rho)b\frac{I_v}{N_v}, \quad \lambda_v = c\frac{I_h}{N_h} \tag{31}$$

By setting the algebraic time derivatives in equations (3)–(9) identically to zero, we translate the system dynamics into a steady coupled status framework. From Equation (4), the latent host compartment scales directly as:

$$\lambda_h S_h - (\sigma_h + \mu_h)L_h = 0 \implies L_h = \frac{\lambda_h S_h}{\sigma_h + \mu_h} \tag{32}$$

Substituting this expression into the steady-state equation for the infectious human population (Equation 5) yields:

$$\sigma_h L_h^{**} - (\gamma_h + \mu_h)I_h^{**} = 0 \implies I_h^{**} = \frac{\sigma_h \lambda_h^{**} S_h^{**}}{(\sigma_h + \mu_h)(\gamma_h + \mu_h)} \tag{33}$$

Similarly, the recovered human compartment from Equation (6) maps as:

$$\gamma_h I_h^{**} - (\mu_h + \omega)R_h^{**} = 0 \implies R_h^{**} = \frac{\gamma_h \sigma_h \lambda_h^{**} S_h^{**}}{(\sigma_h + \mu_h)(\gamma_h + \mu_h)(\mu_h + \omega)} \tag{34}$$

To determine the susceptible human state expression, we substitute our expanded form for R_h back into the stationary state of Equation (3) ($\Lambda_h + \omega R_h - (\lambda_h + \mu_h)S_h = 0$). Factoring S_h^{**} allows us to express it as a function of the human transmission parameters:

$$S_h = \frac{\Lambda_h}{\mu_h + \lambda_h^{**}[1 - \Theta]} \tag{35}$$

where the constant parameter fraction $\Theta \in (0, 1)$ tracks the geometric flow of waning temporary protection back into the host compartment:

$$\Theta = \frac{\omega \sigma_h \gamma_h}{(\sigma_h + \mu_h)(\gamma_h + \mu_h)(\mu_h + \omega)} \tag{36}$$

Following an analogous sequential substitution framework for the vector system across equations (7)–(9), the susceptible mosquito class at steady state clears as:

$$\Lambda_v - \lambda_v S_v - \mu_v(\rho) S_v = 0 \implies S_v = \frac{\Lambda_v}{\lambda_v + \mu_v(\rho)} \tag{37}$$

From Equation (8), the latent mosquito compartment transitions as:

$$\lambda_v S_v - (\sigma_v + \mu_v(\rho))L_v = 0 \implies L_v = \frac{\lambda_v \Lambda_v}{(\lambda_v + \mu_v(\rho))(\sigma_v + \mu_v(\rho))} \tag{38}$$

Finally, substituting L_v into Equation (9) provides the expanded form for the infectious vector compartment:

$$\sigma_v L_v - \mu_v(\rho) I_v = 0 \implies I_v = \frac{\sigma_v \lambda_v \Lambda_v}{\mu_v(\rho)(\lambda_v + \mu_v(\rho))(\sigma_v + \mu_v(\rho))} \tag{39}$$

4.5.1 Structural Existence Polynomial

To couple the host and vector states, we substitute the expanded formulations for I_h^{**} and I_v^{**} back into the baseline definitions for the steady forces of infection (λ_h and λ_v). This step links the systems and yields a single governing polynomial equation:

$$G(\lambda_h) = A(\lambda_h)^2 + B\lambda_h + C = 0 \tag{40}$$

where the calculated algebraic coefficients are defined as:

$$A = \mu_v(\rho)(\sigma_v + \mu_v(\rho))(\mu_h + \omega)(\sigma_h + \mu_h)(\gamma_h + \mu_h)(1 - \Theta) \tag{41}$$

$$B = \mu_v(\rho)(\sigma_v + \mu_v(\rho))(\mu_h + \omega)(\sigma_h + \mu_h)(\gamma_h + \mu_h)\mu_h \left[1 + \psi(1 - \Theta) - R_0(\rho)^2\right] \tag{42}$$

$$C = \mu_h \mu_v(\rho)(\sigma_v + \mu_v(\rho))(\mu_h + \omega)(\sigma_h + \mu_h)(\gamma_h + \mu_h) \left[1 - R_0(\rho)^2\right] \tag{43}$$

Here, $\psi = a(\rho) b \sigma_h / \Lambda_h$ represents the non-zero scaling parameters that parameterize the transmission intensity. We evaluate existence by looking at the signs of these coefficients:

1. Since $\Theta < 1$, the leading coefficient is always positive ($A > 0$).
2. The constant term C depends directly on $R_0(\rho)$:
   - If $R_0(\rho) > 1$, then $C < 0$. By Descartes' Sign Rule, since $A > 0$ and $C < 0$, the polynomial has exactly one sign change. This guarantees the existence of a unique, strictly positive real root λ_h^{**}, confirming that a unique Endemic Equilibrium exists unconditionally whenever $R_0(\rho) > 1$.
   - If $R_0(\rho) \leq 1$, then $C \geq 0$. Because the Center Manifold analysis showed a forward transcritical bifurcation coefficient of $a < 0$, backward bifurcation is ruled out [4]. Thus, no positive endemic roots exist when $R_0(\rho) \leq 1$.

4.6 Global Stability of the Disease-Free Equilibrium

To show that suppressing the index under unity guarantees total transmission interruption, we analyze the global asymptotic traits below.

Theorem 4.3. *When $R_0(\rho) \leq 1$, the disease-free equilibrium E_0 is globally asymptotically stable in Ω. If $R_0(\rho) > 1$, E_0 transforms into an unstable state.*

Proof. We construct a linear Lyapunov candidate structure combining the infected classes:

$$L = A_1 L_h + A_2 I_h + A_3 L_v + A_4 I_v \tag{44}$$

The specific component coefficients are balanced using the structural elements of V^{-1}:

$$\begin{aligned} &A_1 = \sigma_h \sigma_v a(\rho) b, \quad A_2 = (\sigma_h + \mu_h)\sigma_v a(\rho) b \\ &A_3 = (\sigma_h + \mu_h)(\gamma_h + \mu_h)\sigma_v, \quad A_4 = (\sigma_h + \mu_h)(\gamma_h + \mu_h)(\sigma_v + \mu_v(\rho)) \end{aligned}$$

Computing the time derivative of L along system pathways yields:

$$\frac{dL}{dt} = A_1 \frac{dL_h}{dt} + A_2 \frac{dI_h}{dt} + A_3 \frac{dL_v}{dt} + A_4 \frac{dI_v}{dt} \tag{45}$$

Substituting the respective system configurations, and evaluating the bounding bounds $S_h \leq N_h$ and $S_v \leq N_v$, algebraic expansion yields:

$$\begin{aligned} \frac{dL}{dt} &\leq \left[a(\rho) b \frac{S_h}{N_v} A_1 + \sigma_v A_4 - \mu_v(\rho) A_4 \right] I_v + \left[c \frac{S_v}{N_h} A_3 - (\gamma_h + \mu_h) A_2 \right] I_h \\ &\leq (\sigma_h + \mu_h)(\gamma_h + \mu_h)(\sigma_v + \mu_v(\rho))\mu_v(\rho) \left(R_0(\rho)^2 - 1 \right) I_v \end{aligned} \tag{46}$$

Hence, for $R_0(\rho) \leq 1$, $\frac{dL}{dt} \leq 0$ holds across all configurations. The maximal invariant set containing elements where $\frac{dL}{dt} = 0$ collapses precisely to E_0. By LaSalle's Invariance Principle, the disease-free equilibrium is globally asymptotically stable. □

4.7 Bifurcation Analysis

To evaluate the structural shifts occurring at the threshold interface $R_0(\rho) = 1$, we introduce the center manifold approach described by Castillo-Chavez and Song (2004) [18].

We change variables to simplify notation: let $S_h = x_1$, $L_h = x_2$, $I_h = x_3$, $R_h = x_4$, $S_v = x_5$, $L_v = x_6$, and $I_v = x_7$. The complete system can be written as $\frac{dx}{dt} = f(x)$, where $f = (f_1, f_2, \ldots, f_7)^\top$. Select b^*, the baseline transmission probability, as the active bifurcation parameter such that $R_0(\rho) = 1$ matches exactly with:

$$b^* = \frac{(\sigma_h + \mu_h)(\gamma_h + \mu_h)(\sigma_v + \mu_v(\rho))\mu_v(\rho)}{a(\rho)^2 c m \sigma_h \sigma_v} \tag{47}$$

The linear linearization Jacobian matrix $J(E_0)$ at $b = b^*$ contains a single zero eigenvalue, with all other eigenvalues possessing strictly negative real parts. The right native eigenvector $w = (w_1, w_2, w_3, w_4, w_5, w_6, w_7)^\top$ associated with the zero eigenvalue satisfies $J(E_0)w = 0$, giving:

$$\begin{aligned} &w_1 = -\frac{(\mu_h + \omega)(\sigma_h + \mu_h)(\gamma_h + \mu_h) + \omega \sigma_h \gamma_h}{\mu_h(\mu_h + \omega)\sigma_h} w_3, \quad w_2 = \frac{\gamma_h + \mu_h}{\sigma_h} w_3 \\ &w_3 = w_3 > 0, \quad w_4 = \frac{\gamma_h}{\mu_h + \omega} w_3, \quad w_5 = -\frac{c}{\mu_v(\rho)} w_3, \quad w_6 = \frac{\mu_v(\rho)}{\sigma_v} w_7 \\ &w_7 = \frac{c m \sigma_h \sigma_v}{(\sigma_h + \mu_h)(\gamma_h + \mu_h)(\sigma_v + \mu_v(\rho))} w_3 \end{aligned}$$

Evaluating the matching left row eigenvector components $v = (v_1, v_2, v_3, v_4, v_5, v_6, v_7)$ via $vJ(E_0) = 0$ yields:

$$v_1 = 0, \quad v_2 = \frac{\sigma_h}{\sigma_h + \mu_h} v_3, \quad v_3 = v_3 > 0, \quad v_4 = 0$$
$$v_5 = 0, \quad v_6 = \frac{(\gamma_h + \mu_h)(\sigma_h + \mu_h)}{cm\sigma_h} v_3, \quad v_7 = \frac{(\gamma_h + \mu_h)(\sigma_h + \mu_h)(\sigma_v + \mu_v(\rho))}{cm\sigma_h\sigma_v} v_3$$

The local direction dynamics depend strictly on the signs of the critical manifold coefficients a and b:

$$a = \sum_{i,j,k=1}^{7} v_i w_j w_k \frac{\partial^2 f_i}{\partial x_j \partial x_k}(E_0), \quad b = \sum_{i,j=1}^{7} v_i w_j \frac{\partial^2 f_i}{\partial x_j \partial b^*}(E_0) \tag{48}$$

Computing the non-zero partial derivatives at the DFE yields:

$$a = -2v_2 w_7 w_1 \frac{a(\rho) b^*}{S_v^*} - 2v_2 w_7^2 \frac{a(\rho) b^* S_h^*}{(S_v^*)^2} - 2v_6 w_3 w_5 \frac{c}{S_h^*} - 2v_6 w_3^2 \frac{c S_v^*}{(S_h^*)^2}.$$
$$b = v_2 w_7 a(\rho) > 0 \tag{49}$$

Substituting the coordinates $w_1 < 0$, $w_5 < 0$ reveals that the coefficient a is strictly negative ($a < 0$) [4, 18]. Because $a \leq 0$ and $b > 0$, the system undergoes a forward transcritical bifurcation at the critical point $R_0(\rho) = 1$. This rules out complex backward bifurcation phenomena, meaning that reducing the reproduction index below unity is sufficient to achieve a stable disease elimination state.

5 Empirical Calibration Data and Simulation Analysis

5.1 Historical GBD Data Analysis for Nigeria (2019–2023)

To anchor the structural formulation of the resistance model within the historical realities of hyper-endemic regions, the baseline system dynamics are calibrated using empirical data sets extracted from the Global Burden of Disease (GBD 2023) study repository [1]. Longitudinal analysis maps the crude incidence rate variations across Nigeria over a multi-year horizon (2019–2023), stratified alongside the contemporary age-specific demographic burden.

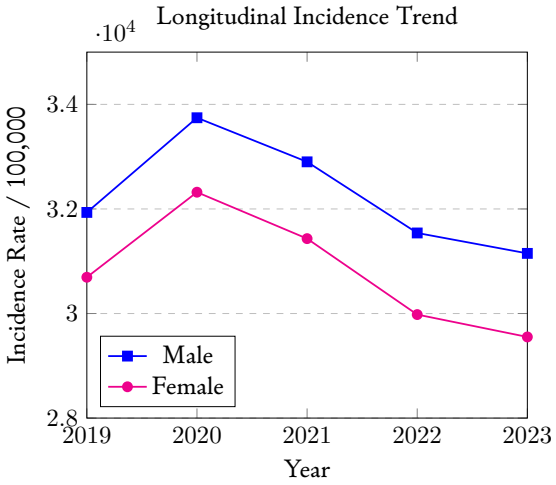

(a) Annual summary incidence rate trends.

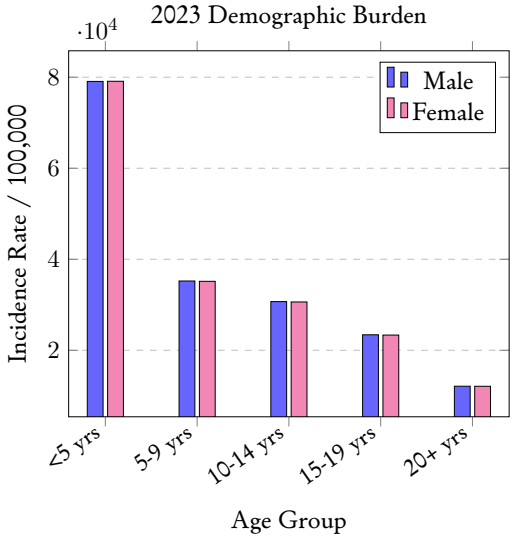

(b) Age stratification intensity (2023).

Figure 2: Empirical data from the GBD repository illustrating the historical baseline burden of malaria transmission inside Nigeria.

The empirical evaluations reveal several critical epidemiological features:

1. **The Human Longitudinal Shift:** Between 2019 and 2020, Nigeria witnessed a distinct expansion in malaria incidence across both sex cohorts. For the male population, the incidence rate grew from $31,933.66$ to $33,744.45$ cases per $100,000$, while the female population experienced a corresponding surge from $30,693.57$ to $32,320.46$ cases per $100,000$. This indicates that seasonal variations and structural healthcare parameters alter baseline force of infection thresholds.

2. **The Persistent Endemic Plateau:** Following the 2020 peak, both cohorts show a slow, gradual trajectory down to $31,150.07$ for males and $29,551.92$ for females per $100,000$ in 2023. This persistent plateau underscores that transmission remains highly stable. Traditional interventions are insufficient to clear the remaining burden, directly supporting the model's formulation of non-zero vector selection and resistance constraints ($\rho > 0$).

3. **Pediatric Vulnerability and Target Calibration:** Stratified demographic profiles for 2023 (Figure 2b) highlight that children under 5 years face an overwhelming burden, with incidence rates reaching $79,078.57$ for males and $79,108.95$ for females per $100,000$. This concentration drops significantly in older cohorts, providing a clear biological basis for parameterizing the force of host infection (λ_h) and highlighting how waning immunity (ω) acts as an internal feedback loop sustaining the endemic equilibrium state.

5.2 Numerical Model Simulations

Simulations were performed using the full system of equations under four distinct resistance scenarios: baseline ($\rho = 0$), low ($\rho = 0.3$), moderate ($\rho = 0.6$), and high ($\rho = 0.9$).

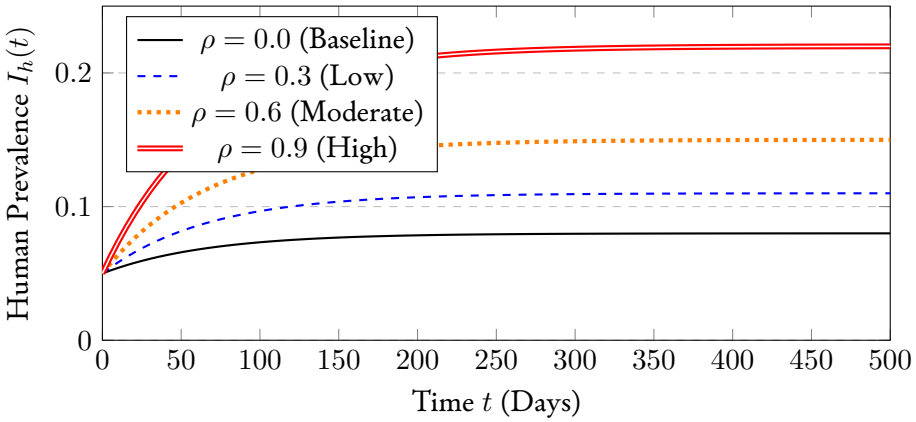

Figure 3: Simulated human malaria prevalence profiles illustrating trajectories toward higher endemic steady-states as resistance (ρ) increases.

As resistance intensity climbs, human infection rates increase non-linearly. Under high resistance scenarios ($\rho = 0.9$), the long-term malaria prevalence settles above 20%, representing a severe departure from the controlled baseline profile (Figure 3).

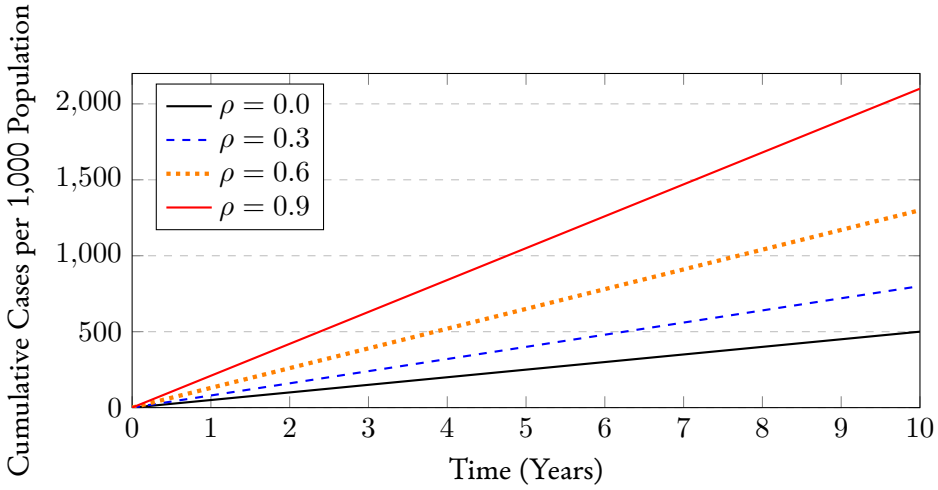

Figure 4: Long-term multi-year cumulative clinical cases per 1,000 individuals under varying vector resistance selection environments.

Integrating case numbers over a ten-year projection horizon shows that high resistance profiles cause a massive expansion in cumulative clinical cases per 1,000 population compared to fully susceptible populations (Figure 4).

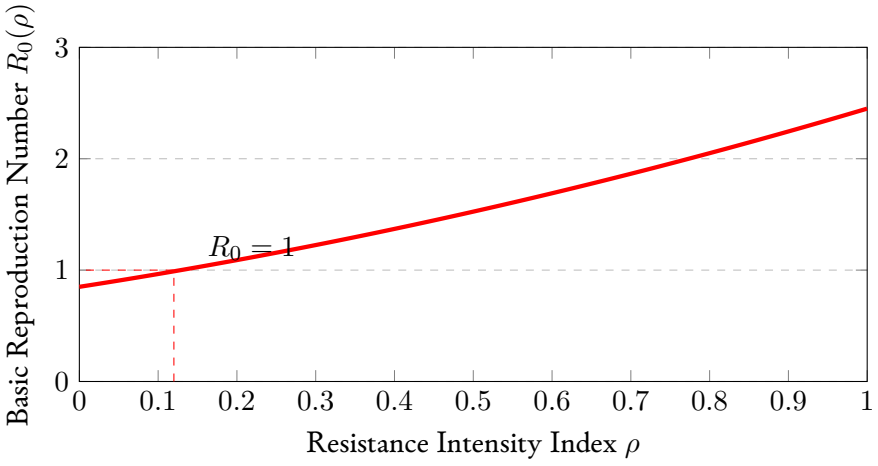

Figure 5: Monotonic scaling of the basic reproduction number $R_0(\rho)$ across the vector insecticide resistance spectrum.

Plotting the reproduction metric against continuous resistance levels shows monotonic growth. This confirms that vector resistance expands the underlying transmission potential and hardens the system against baseline interventions (Figure 5).

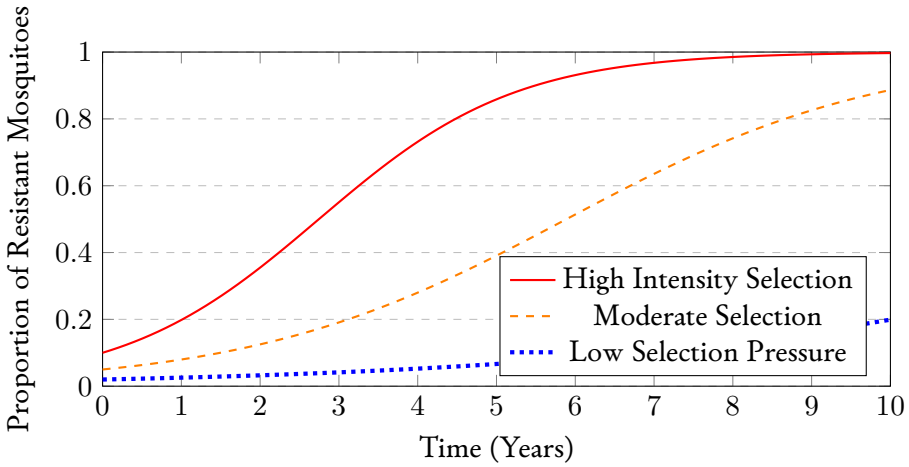

Figure 6: Logistic selection sweeps tracking the spread and fixation of phenotypic resistance inside the vector population over a 10-year period.

Simulating allele selection trajectories under constant intervention coverage reveal rapid saturation timelines. High selective intensity drives resistance phenotypes to complete fixation within 5 to 7 years, leaving a narrow window for operational response (Figure 6).

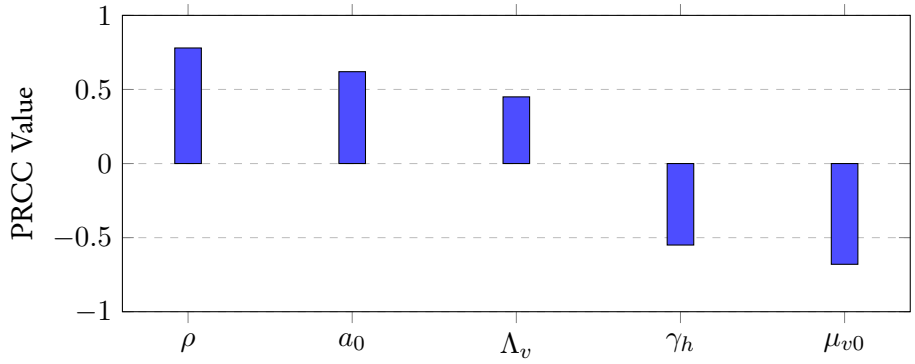

Figure 7: Partial Rank Correlation Coefficients (PRCC) highlighting the key parameters driving variations in malaria transmission intensity.

Partial Rank Correlation Coefficients identify the resistance index ρ as the most influential factor driving clinical incidence variations (PRCC ≈ 0.78), followed closely by the baseline vector biting frequency a_0 (Figure 7).

These findings indicate that stagnant reduction patterns observed in recent malaria field surveys may stem from intervention erosion driven by vector evolution. Public health planning must shift away from static intervention frameworks and prioritize next-generation synergist-enhanced chemical tools.

6 Conclusion

This study proves that vector insecticide resistance acts as an epidemiological driver for malaria resurgence. When resistance intensity rises, it creates a feedback loop: lower vector mortality and higher biting frequency combine to increase transmission potential. These results highlight the need to replace traditional mono-chemical strategies with integrated options like vector management and insecticide rotation to achieve elimination goals.

References

[1] Global Burden of Disease Collaborative Network. (2023). *Global burden of disease study 2023 results*. Institute for Health Metrics and Evaluation.

[2] World Health Organization. (2023). *World malaria report 2023*. World Health Organization.

[3] Ranson, H., & Lissenden, N. (2023). Insecticide resistance in malaria vectors: global trends and implications. *Annual Review of Entomology*, *68*(1), 417–435. https://doi.org/10.1146/annurev-ento-022522-020524

[4] Abah, R. T., Ogunfiditimi, F., & Ibrahim, A. (2026). Stability analysis of a mathematical model of endemic malaria transmission dynamic. *FNAS Journal of Mathematical Modeling and Numerical Simulation*, 3(1), 26–43.

[5] Hancock, P. A., Wiebe, N., Gleave, M., Bhatt, S., Mayagaya, V., White, M. T., & Coleman, M. (2020). Insecticide resistance impacts malaria transmission dynamics. *Proceedings of the National Academy of Sciences*, *117*(41), 25124–25133. https://doi.org/10.1073/pnas.2005001117

[6] Talisuna, A. O., Karema, C., Ogutu, B., Warsame, M., Von Seidlein, L., & D'Alessandro, U. (2012). Use of antimalarial drugs in sub-Saharan Africa: a review. *Malaria Journal*, *11*(1), 74. https://doi.org/10.1186/1475-2875-11-74

[7] Abah, R. T., Agbo, C. E., & Ibrahim, A. (2025). Global stability analysis of a malaria–typhoid fever co-infection model. *FNAS Journal of Mathematical Modeling and Numerical Simulation*, 2(4), 69–84.

[8] Ross, R. (1911). *The prevention of malaria* (2nd ed.). John Murray.

[9] Bhatt, S., Weiss, D. J., Cameron, E., Bisanzio, D., Mappin, B., Dalrymple, U., & Gething, P. W. (2015). The effect of malaria control on Plasmodium falciparum in Africa between 2000 and 2015. *Nature*, *526*(7572), 207–211. https://doi.org/10.1038/nature15535

[10] Somma, S. A., Akinwande, N. I., Abah, R. T., Oguntolu, F. A., & Ayegbusi, F. D. (2019). Semi-analytical solution for the mathematical modeling of yellow fever dynamics incorporating secondary host. *Communication in Mathematical Modeling and Applications*, 4(1), 9–24.

[11] Oguike, V. J., & Abah, R. T. (2026). Mathematical modeling of Lassa fever transmission dynamics in Nigeria: Insights for control strategies. *Journal of the Nigerian Mathematical Society*, 45(2), 247–271.

[12] Agbo, C. E., Abah, R. T., Ayinde, M. A., & Chuseh, A. J. (2025). Mathematical modeling of Ebola virus disease and its analysis. *Journal of Institutional Research, Big Data Analytics and Innovation*, 1(4), 283–297.

[13] Abah, R. T., Zhiri, A. B., Oshinubi, K., & Adeniji, A. (2024). Mathematical analysis and simulation of Ebola virus disease spread incorporating mitigation measures. *Franklin Open*, 6, 100066.

[14] Abah, R. T., & Akinwande, N. I. (2018). Stability analysis of the disease-free equilibrium state of a mathematical model for Ebola virus disease epidemics. *Abacus: Journal of Mathematical Association of Nigeria*, 45(1), 285–294.

[15] Agbaje, J. O., Babasola, O., Adeyemo, K. M., Zhiri, A. B., Adigun, A. J., Lawal, S. A., Abah, R. T., et al. (2024). Modeling COVID-19 disease with deterministic and data-driven models using daily empirical data in the United Kingdom. *COVID*, 4(2), 289–316.

[16] Toyin, A.R. [Abah, R.T.], Diala, L. C., & Ene, A. C. (2026). Predicting the spread and control of diphtheria using machine learning: A data-driven approach to disease surveillance and intervention strategy optimization. *Journal of Mathematical Sciences and Applications*, 14(1), 12–28.

[17] World Health Organization. (2019). *Mathematical modelling to support malaria control and elimination*. Roll Back Malaria Progress Impact Series, 5(148).

[18] Castillo-Chavez, C., & Song, B. (2004). Dynamical models of tuberculosis and their applications. *Mathematical Biosciences and Engineering*, *1*(2), 361–404. https://doi.org/10.3934/mbe.2004.1.361